Nosocomial *Pseudomonas aeruginosa* regulates alginate biosynthesis and Type VI secretion system during adaptive and convergent evolution for coinfection in critically ill COVID-19 patients

Jiuxin Qu[1*], Zhao Cai[2*], Xiangke Duan[2], Han Zhang[2], Shuhong Han[2], Kaiwei Yu[2], Zhaofang Jiang[1], Yingdan Zhang[2], Yang Liu[3], Yingxia Liu[1,4], Lei Liu[1,4#], Liang Yang[2,5#]

1 Department of Clinical Laboratory, Shenzhen Third People's Hospital, Second Hospital Affiliated to Southern University of Science and Technology, National Clinical Research Center for Infectious Diseases, 518000, Shenzhen, Guangdong, China

2 School of Medicine, Southern University of Science and Technology, Shenzhen, 518055, China

3 Medical Research Center, Southern University of Science and Technology Hospital, 518055, Shenzhen, China

4 Shenzhen Key Laboratory of Pathogen and Immunity, State Key Discipline of Infectious Disease, Shenzhen Third People's Hospital, Second Hospital Affiliated to Southern University of Science and Technology, Shenzhen 518112, China

5. Shenzhen Key Laboratory for Gene regulation and Systems Biology, Southern University of Science and Technology, Shenzhen, 518055, China

* These authors contributed equally to this work

[#] These authors contributed equally to this work and share the corresponding authorship

Corresponding authors: Lei Liu (Liulei3322@aliyun.com) and Liang Yang (yangl@sustech.edu.cn)

Running title: *Pseudomonas aeruginosa* evolution in COVID-19 patients

Abstract

COVID-19 pandemic has caused millions of death globally and caused huge impact on the health of infected patients. Shift in the lung microbial ecology upon such viral infection often worsens the disease and increases host susceptibility to secondary infections. Recent studies have indicated that bacterial coinfection is an unignorable factor contributing to the aggravation of COVID-19 and posing great challenge to clinical treatments. However, there is still a lack of in-depth investigation on the coinfecting bacteria in COVID-19 patients for better treatment of bacterial coinfection. With the knowledge that *Pseudomonas aeruginosa* is one of the top coinfecting pathogens, we analyzed the adaptation and convergent evolution of nosocomial *P. aeruginosa* isolated from two critical COVID-19 patients in this study. We sequenced and compared the genomes and transcriptomes of *P. aeruginosa* isolates longitudinally and parallelly for its evolutionary traits. *P. aeruginosa* overexpressed alginate and attenuated Type VI secretion system (T6SS) during coinfection for excessive biofilm formation and suppressed virulence. Results of bacterial competition assay and macrophage cytotoxicity test indicated that *P. aeruginosa* reduced its virulence towards both prokaryotic competitors and eukaryotic host through inhibiting its T6SS during evolution. *P. aeuginosa* T6SS is thus one of the reasons for its advantage to cause coinfection in COVID-19 patients while the attenuation of T6SS could cause a shift in the microecological composition in the lung. Our study will contribute to the development of therapeutic measures and the discovery of novel drug target to eliminate *P. aeruginosa* coinfection in COVID-19 patient.

Introduction

Coronavirus Disease 2019 (COVID-19) induced by Severe Acute Respiratory Syndrome Coronavirus 2 (SARS-CoV-2) has caused over 2.8 million death globally as reported by WHO at Apr 2021. SARS-CoV-2 induces cytokine storm and hyperinflammation resulting in respiratory dysfunction and necrosis of epithelial cells of the lungs [1, 2]. Such histological changes in the lung tissues may result in dysbiosis of lung microbiome and give rise to secondary bacterial infection in COVID-19 patients [3]. Several groups of researchers have emphasized that microbial coinfection indeed occurs in COVID-19 patients, especially in severe cases, exacerbates disease progress and makes difficulties to clinical treatments [4-7].

Nosocomial bacterial pathogens are risk factors contributing to such microbial coinfections and resulting in increased death of critically ill COVID-19 patients [8, 9]. Bacterial coinfection in COVID-19 patients is a serious problem which should not be neglected. The common coinfecting bacteria reported include *Mycoplasma pneumonia*, *Staphylococcus aureus*, *Klebsiella spp., Acinetobacter baumannii, Haemophilus influenzae*, *Pseudomonas aeruginosa* and etc [10, 11]. There was bacteremia case caused by *Pseudomonas* reported [12]. *P. aeruginosa* is identified as a top coinfecting bacteria in our hospital (unpublished data).

Pseudomonas aeruginosa is a well-known nosocomial pathogen causing fatal chronic infections in immunocompromised patients with diseases like cystic fibrosis, catheter-associated infections and burn wounds [13, 14]. This bacterium induces infections through different mechanisms, including biofilm formation, quorum sensing systems and secretion of virulence factors [13]. *P. aeruginosa* possesses diverse virulence systems including quorum sensing systems, protein secretion systems, lipopolysaccharides etc for competition in the polymicrobial environments

and invasion to host cells[13]. Longitudinal analysis of convergent evolution of *P. aeruginosa* clinical isolates indicated that remodeling of virulence secretion is essential for host adaptation [15, 16]. Mutations in genes, *mucA, vgrG, lasR, rpoN* and *pvdS,* significantly impair quorum sensing systems, protein secretion systems and virulence factor biosynthesis allowing *P. aeruginosa* to escape from host immune clearance in patients with lung diseases such as cystic fibrosis and ventilator-associated pneumonia [15-18]. Among the secretion systems, Type VI secretion system (T6SS) highly correlates to bacterial competition and host interaction of *P. aeruginosa* with other organisms [19]. Analysis of these evolutionary traits could contribute to the development of therapeutic measures to treat infections caused by *P. aeruginosa*. However, there is still a paucity of data on the insight of nosocomial *P. aeruginosa* coinfection with SARS-CoV-2 virus and its evolution during coinfection. To address this, we sequenced and compared the genomes and transcriptomes of four *P. aeruginosa* isolates sampled longitudinally from two critically ill COVID-19 patients to investigate its adaptive convergent evolution. The isolates collected from different patients are of the same sequence typing indicating the occurrence of hospital-acquired *P. aeruginosa* infection. The results showed that these isolates form excessive biofilm by developing mucoid phenotype through increasing alginate biosynthesis for long-term colonization in the host. More notably, we demonstrated here that *P. aeruginosa* evolves and attenuates its T6SS, especially HSI-II T6SS, to suppress its virulence to escape host clearance during coinfection. Understanding such adaptive convergent evolution could contribute to the treatment decision and the discovery of novel drug target to eliminate *P. aeruginosa* infection in COVID-19 patients.

Material and Methods

Isolate collection, bacterial strains and growth media

Four isolates of *Pseudomonas aeruginosa* were collected at two different time points longitudinally from sputum samples or bronchioalveolar lavage fluids (BALF) of two critically ill COVID-19 patients respectively during routine clinical tests. Isolates collected from patient 1 were named as LYSZa2 and LYSZa3 while isolates collected from patient 2 were named as LYSZa5 and LYSZa6. Luria-Bertani (LB) broth and ABTGC medium supplemented with 10% Tryptic Soy Broth (TSB) were used for growing cultures. ABTGC medium consists of 0.1% $MgCl_2$, 0.1% $CaCl_2$, 0.1% $FeCl_3$, 0.2% glucose, 0.2% casamino acids and 10% A10 medium which is made of 15.1mM $(NH_4)_2SO_4$, 33.7mM $Na_2HPO_4 \cdot 2H_2O$, 22 mM KH_2PO_4 and 0.05mM NaCl.

Ethical statement

This work does not include any direct participation of the patients and does not contain any identifiable human data. This work is approved by the Ethics Committee of Shenzhen Third People's Hospital, Second Hospital Affiliated to Southern University of Science and Technology [2020-184] and filed with the Ethics Committee of Southern University of Science and Technology [20200069].

Antimicrobial susceptibility tests

Antimicrobial susceptibility of the isolates to various antibiotics, including ceftazidime, piperacillin, cefoperazone/sulbactam, imipenem, aztreonam, and levofloxacin, were performed using the Kirby-Bauer disc-diffusion method. Diameters of inhibition zone was measured using a vernier caliper. Susceptibility was determined according to CLSI 2019[20]. Results of antibiotic susceptibility tests were listed in Table S1.

Biofilm formation assay

The isolates were cultured in LB broth at 37°C for overnight. The overnight cultures were diluted to OD_{600nm} 0.01 in fresh LB broth. 100µL of the diluted cultures were loaded into 96-well plate in triplicates and incubated for 24h at 37°C statically allowing the formation of biofilm. After removing spent media, biofilms were washed carefully with ddH_2O for two times. Biofilms were then stained by 125 µL of 0.1% crystal violet (CV) with 15 min incubation at room temperature. CV stain in the wells was discarded while stained biofilms were washed twice thoroughly with ddH_2O and air-dried. Biofilms were then dissolved into 125 µL of 30% acetic acid and quantified relatively by measuring OD_{550nm} values on a Tecan infinity pro200 microplate reader.

Genome extraction and sequencing

The isolates were cultured in LB broth at 37°C to early stationary phase. For Illumina sequencing, genomic DNA of each isolates was extracted using AxyPerp Bacterial Genomic DNA Miniprep Kit (Corning, New York, USA) following manufacturer's protocol. PCR-free libraries were constructed using VAHTSTM PCR-Free DNA Library Prep Kit for Illumina® (Vazyme, China) following standard protocol. VAHTSTM DNA Adapters for Illumina® (Vazyme, China) was used to tag adaptor to purified fragments. Quality of the libraries were assessed by Agilent Technologies 2100 Bioanalyzer and qPCR. Paired-end DNA sequencing was then performed on Illumina HiSeq X platform with read length of 150 bp. For PacBio sequencing, genomes of LYSZa2 and LYSZa5 were extracted using Mabio Bacterial DNA Extraction Mini Kits (Mabio) according to manufacturer's protocol. DNA fragmentation was done using G-tubes (Covaris). SMRTbell DNA template libraries were prepared according to the manufacturer's specification (PacBio, Menlo Park, USA). DNA sequencing was then performed on Pacific Biosciences RSII sequencer (PacBio, Menlo Park, USA).

Transcriptome extraction and sequencing

The isolates were cultured in triplicates in LB broth at 37°C to early stationary phase. Magen HiPure Universal RNA Mini kits (MCBio, China) was used to extract total RNA following the manufacturer's protocol. Extracted RNA was quantified using Qubit 2.0 (Thermo Fisher Scientific, MA, USA) and Nanodrop One (Thermo Fisher Scientific, MA, USA). Quality of RNA samples was assessed by Agilent 2100 system (Agilent Technologies, Waldbron, Germany). RNA libraries were constructed according to standard protocol using NEB Next® Ultra™ Directional RNA Library Prep Kit for Illumina® (New England Biolabs, MA, USA). Ribosomal RNA depletion was carried out using Ribo-zero rRNA Removal Kit. cDNA was synthesized using NEB Next First Strand Synthesis Reaction Buffer. Paired-end RNA sequencing was performed on Illumina NovaSeq 6000 platform with read length of 150 bp.

Sequencing data analysis

Genomic Illumina sequencing reads were assembled into contigs using De Novo Assembly module of CLC Genomics Workbench 20 (Qiagen) with default parameters. Single nucleotide polymorphism was detected using 'Resequencing' module of CLC Genomics Workbench 20 based on frequency of more than 80% using *P.aeruginosa* PAO1 genome as reference. PacBio sequencing reads were assembled into draft genome using HGAP4 pipeline of SMRT Link software v9.0 with default settings. Rearrangements of draft genomes were checked using Mauve software v.2.4.0 by PROGRESSIVEMAUVE alignment mode[21]. Multilocus sequence typing (MLST) was performed using MLST service available on the Center of Genomic of Epidermiology (CGE) webserver[22]. Identification of antimicrobial resistance genes was performed using ResFinder service on CGE webserver based on 85% of identity and 60% of minimal length[23]. Phylogenetic tree was constructed using Parsnp under libMUSCLE aligment mode using draft genomes of the isolates and other strains [24]. Genomic islands on LYSZa2 and

LYSZa5 genomes were predicted using IslandViewer 4 webservice [25]. Circular plot was constructed using BLAST Ring Image Generator [26]. Genomic loci were visualized using Easyfig package[27]. Gene names on the genomic loci were obtained from Pseudomonas Genome Database[28]. Prediction of protein functions of the genes were performed using NCBI Prokaryotic Genome Annotation Pipeline (PGAP) [29].

RNA sequences were pre-processes, mapped to *P. aeruginosa* PAO1 reference genome and analyzed using RNA analysis module of CLC Genomics Workbench 20 (Qiagen) with default parameters. Total read counts of each sample were normalized and compared using DESeq2 R package. Differentially expressed genes (DEGs) were selected based on absolute fold change□4, adjusted p-value<0.05 and base mean □ 20 [30]. GO enrichment analysis of DEGs was performed on DAVID bioinformatics database v6.8 [31]. PCoA plot and heatmap were drawn using Vegan, ggplot2, and pheatmap packages in R 4.0.0.

Bacterial competition assay

Competition between *P. aeruginosa* and *Escherichia coli* was carried out following the steps described previously by Hachani.et.al[32]. Briefly, the isolates were cultured overnight at 37°C on LB agar plates. *E. coli/pLacZ* strain was grown on LB agar plates containing 40 mg/mL of 5-bromo-4-chloro-indolyl-β-D-galactopyranoside (X-gal) at 37°C for overnight and appeared blue in colour. Single colony of each strain was subcultured in TSB medium and grown under agitation for overnight. Appropriate volume of each overnight culture was taken to make final OD600nm =1 and centrifuged to collect cells. Cell pellets were resuspended in 100 µL TSB medium while 10 µL of each suspension was spotted and incubated on LB agar plate for 5 hours at 37°C. 30 µL of cell suspension of each *P. aeruginosa* strain was taken and mixed gently with 30 µL of *E. coli* cell suspensions. 20 µL of mixed cell cultures were spotted onto LB agar plate

and incubated for 5 hours at 37°C. Each bacterial spot was scraped from LB agar plates and resuspended in 1mL of TSB medium. Resuspensions of bacterial spots were diluted to 10^{-3} serially in 10-fold dilutions. These serial cell dilutions were then spotted in triplicates onto LB agar plates containing 40 mg/mL X-gal and incubated for 8 hours for killing *E. coli*. 100 µL of 10^{-3} dilution of each mixed bacterial spot were plated onto LB agar plates containing 40 mg/mL X-gal for CFU counting of *E. coli* for quantitating killing effect.

Cytotoxicity assay

The cytotoxicity of the isolates was assayed by using murine RAW 264.7 macrophages. RAW macrophages were grown in 24-well plates in Dulbecco modified Eagle medium (DMEM), GlutaMAX, sodium pyruvate, and phenol red supplemented with 10% FBS. Prior to infection, confluent RAW cells were washed twice with sterile PBS and incubated in DMEM medium. Log-phase cultures were washed with sterile PBS twice, and resuspended in DMEM medium devoid of FBS. Macrophage cells were infected with the isolates respectively at a Multiplicity of Infection (MOI) of 20 at 37 ℃ in 5% CO2 incubator. After 3 h infection, the culture supernatants were collected for detecting lactate dehydrogenase (LDH) activities. The LDH activities were detected by using commercially LDH cytotoxicity kit (YAESEN Bio) according to standard procedure.

Data Availability

All Illumina sequencing data used in this study could be found from BioProject No. PRJNA706783 and assembled genomes of *P. aeruginosa* LYSZa2 and *P. aeruginosa* LYSZa5 could be found from BioProject No. PRJNA712958 and PRJNA712961 on NCBI.

Results

Hospital-acquired *P. aeruginosa* in the respiratory systems of COVID-19 patients

During routine screening of respiratory samples of COVID-19 patients, we discovered that two patients were colonized by *P. aeruginosa* with the same ST type. We have identified and isolated *P. aeruginosa* from 5 different critically ill patients in total. To investigate genetic adaptation and epidemiological link between these *P. aeruginosa* isolates, genomes of all isolates were sequences by Illumina HiSeq platform. Multi-Locus Sequence Typing (MLST) analysis indicated that four isolates collected from 2 patients are of the same type, *P. aeruginosa* ST1074, showing that these *P. aeruginosa* isolated from these two patients were hospital-acquired. We thus focused on these isolates to analyze their competitive advantage during colonization in COVID-19 environment. These four *P. aeruginosa* isolates were collected from respiratory samples of the two patients and named as LYSZa2, LYSZa3, LYSZa5 and LYSZa6 respectively. Among which, LYSZa2 and LYSZa3 were isolated from patient 1 with 3 days interval while LYSZa2 was isolated on day 12 of hospitalization. LYSZa5 and LYSZa6 were isolated from patient 2 with 15 days interval while LYSZa5 was isolated on day 17 of hospitalization. Genomes of the first isolate of each patient, LYSZa2 and LYSZa5, were further sequenced using Pacific Biosciences RSII sequencer for further analysis. We defined LYSZa2 and LYSZa5 as the ancestry isolates while LYSZa3 and LYSZa6 as the progeny isolates, and analyzed their general genomic characteristics.

Characterization of LYSZa2 and LYSZa5 genomes, phylogeny and antibiotic resistance

Circular genomes of LYSZa2 and LYSZa5 were assembled with genome sizes of 6 638 980 bp and 6 638 990 bp, with 66.2% of GC respectively. Rearrangements were checked and manually curated after pairwise comparison of the two genomes. As predicted by PGAP, LYSZa2 genome contains 6183 genes among which 6046 features encode for proteins and 86 encode for RNAs,

while LYSZa5 genome contains 6183 genes among which 6045 features encode for proteins and 86 encodes for RNAs.

Both of the genomes contain the same antimicrobial resistance genes predicted by ResFinder, including *crpP*, *aph(3')-IIb*, *catB7*, *blaOXA-50*, *blaPAO*, and *fosA* against Fluoroquinolone, Aminoglycoside, Phenicol, Beta-lactam and Fosfomycin drugs. No difference in antimicrobial genes was identified between the ancestry and the progeny isolates. *In vitro* antimicrobial resistance of the isolates were tested using antibiotics including ceftazidime, piperacillin, cefoperazone/sulbactam, imipenem, aztreonam and levofloxacin. Obvious differences in resistance were observed between the ancestry and the progeny isolates. LYSZa5 is sensitive to imipenem, aztreonam and levofloxacin. However, LYSZa6 becomes resistance to imipenem, aztreonam and intermediate to levofloxacin after 15 days of evolution (Table S1). No obvious change in resistance to these drugs was observed between LYSZa2 and LYSZa3 probably due to the short evolving time (Table S1).

Genomic islands (GIs) on LYSZa2 and LYSZa5 genomes were predicted by IslandViewer4 (Table S2&S3). In total, 35 GIs on LYSZa2 and 36 GIs on LYSZa5 were predicted by at least one prediction method. Genomes of LYSZa2 and LYSZa5 were compared with genomes of five other *P. aeruginosa* strains including PAO1 reference strain and virulence strains including PA14, LESB58, SCV20265 and VFRPA04 (Figure 1A). Most of the GIs predicted are specific to LYSZa2 and LYSZa5 genomes (Figure 1A). Genes in these GIs are involved in transcriptional regulation, DNA restriction-modification, DNA repair, toxin-antitoxin and secretion systems, showing that these GIs are essential for *P. aeruginosa* survival and virulence during coinfection with SARS-CoV-2.

We then traced the origin of these isolates by constructing phylogenetic tree using genomes of

LYSZa2 and LYSZa5 with 22 other clinical or environmental *P. aeruginosa* genomes selected from NCBI/Pseudomonas genome database (Table S4) and one SARS-CoV-2 coinfecting strain published by our group recently, *P. aeruginosa* LYSZa7[33]. As seen from the phylogenetic tree (Figure 1B), LYSZa2 and LYSZa5 are closed related without evolutionary distance between them, and are in the same phylogenetic cluster with PAO1 reference strain and the hypervirulent isolate LESB58 from CF patient. Interestingly, great evolutionary distance was observed between these two isolates with *P. aeruginosa* LYSZa7, indicating the distinct evolutionary traits evolved between different *P. aeruginosa* strains in COVID-19 patients for adaptation.

Single nucleotide polymorphism (SNP) and other genome modifying events were assessed between the ancestry isolates and the progeny isolates respectively using PAO1 as reference (Table S5). 90 genomic modifying events including SNPs, insertion, deletion and replacement (Table S5) were identified in LYSZa3 with a dN/dS ratio of 0.875, indicating a negative selection during evolution, probably due to the short evolving time between these two isolates. 93 of such genomic modifying events (Table S5) were identified in LYSZa6 comparing to LYSZa5 with a dN/dS ratio of 1.114 indicating a positive selection. Common mutations were found between LYSZa3 and LYSZa6 on genes related to Type VI secretion system and iron transport (Table 1). Such observation indicated that *P. aeruginosa* undergoes both adaptive evolution and convergent evolution in COVID-19 patients to survive and modulate its virulence during coinfection. We then performed RNA sequencing to assess the changes at transcriptional level during evolution.

Alginate overproduction and attenuated expression of T6SS during evolution

To discover the transcriptional changes during adaptive evolution, we performed RNA sequencing of the isolates on Illumina HiSeq platform and analyzed differential gene expression between the ancestry isolates and the progeny isolates longitudinally. Moreover, we also

compared the gene expression in parallel between the progeny cells from the two patients to learn the convergent changes of *P. aeruginosa* in different hosts. Based on the filtering criteria of fold change ≥ 4, adjusted p-value<0.05 and base mean ≥ 20, the expression of 129 genes were differentially regulated in LYSZa3 comparing to LYSZa2, among which 75 were upregulated and others were downregulated (Table S6). In LYSZa6 as comparing to LYSZa5, 242 genes were differentially expressed, among which 114 were upregulated and others were downregulated (Table S7). These differentially expressed genes are illustrated by heatmaps (Figure 2A&B), which display distinctive transcriptomic profiles of the progeny isolates comparing to the ancestry isolates. We further clustered the isolates using Principal Coordinates Analysis (PCoA) based on Bray Curtis dissimilarity to check the differences between isolates. As seen from PCoA plots (Figure 2C&D), LYSZa2 group and LYSZa5 group separated clearly from LYSZa3 group and LYSZa6 group respectively, indicating the ancestry isolates and the progeny isolates possessing distinct physiology.

We then performed Gene Ontology (GO) enrichment analysis using the differentially expressed genes (DEGs) to identify highly enriched functions in the progeny isolates comparing to the ancestry isolates (Figure 3). 11 GO consisting of 7 biological processes, 3 molecular functions and 1 cellular component were enriched in LYSZa3 comparing to LYSZa2 (Figure 3A). Whereas in LYSZa6 comparing to LYSZa5, 13 GO consisting of 7 biological processes, 5 molecular functions and 1 cellular component were highly enriched (Figure 3C). Among all of these enriched functions in both the progeny isolates, most significantly enriched biological processes are alginic acid biosynthetic process and protein secretion by the type VI secretion system (T6SS). 12 genes assigned to alginic acid biosynthetic process (*algD*, *algX*, *algA*, *algE*, *algF*, *algL*, *alg44*, *algJ*, *algK*, *alg8*, *algI*, *algG*) were all upregulated in LYSZa3 for 16.89 to 1091.52

295 folds (Table 2). The expression of same genes also increased significantly in LYSZa6 for 4.45 to
296 138.79 folds (Table 3). Eight genes assigned to protein secretion by T6SS, PA1657 (*hsiB2*),
297 PA1658 (*hsiC2*), PA1659 (*hsiF2*), PA1660(*hsiG2*), PA1661(*hsiH2*), PA1662(*clpV2*),
298 PA1663(*sfa2*), PA1666(*lip2*), were all significantly downregulated in LYSZa3 for 4.46 to 6.47
299 folds (Table 2). In LYSZa6, beside the same eight genes mentioned above, 7 other genes
300 assigned to protein secretion by T6SS were also downregulated, including PA1656 (*hsiA2*),
301 PA1665 (*fha2*), PA1667 (*hsiJ2*), PA1668 (*dotU2*), PA1669 (*icmF2*), *stk1* and *stp1*, for 4.46 to
302 17.11 folds (Table 3). Besides these genes assigned to T6SS by GO enrichment analysis, the
303 expression of several other genes involved in T6SS, *hcpB*, *lip3* (PA2364), and *dotU3* (PA2362),
304 were also decreased in LYSZa3 (Table 2). While the expression of 15 other genes involved in
305 T6SS significantly decreased in LYSZa6, including *clpV1*, PA3904(PAAR4), PA2702(*tse2*),
306 PA2774(*tse4*), PA2775(*tsi4*), *vgrG1*, PA0093(*tse6*), PA3905(*tecT*), PA0082(*tssA1*), PA2703(*tsi2*),
307 PA0094(*eagT6*), PA3484(*tse3*), PA5266(*vgrG6*), *hcpA* and *hcpB* (Table 3). *P. aeruginosa* carries
308 three types of T6SS, HSI-I, HSI-II and HSI-III respectively. As illustrated in Figure 4, the
309 downregulated genes in both progeny isolates, especially those in LYSZa6, are mostly involved
310 in HSI-II gene cluster, with several others scattered on another two gene clusters. Higher no. of
311 DEGs observed in LYSZa6 comparing to LYSZa3 may consequently due to the longer evolving
312 time of LYSZa6 in the host. The changes in the gene abundance assigned to different GO
313 functions are illustrated in Figure 3B&D. There was dramatic increase in the gene abundance for
314 alginic acid biosynthetic process and significant decrease in the gene abundance for protein
315 secretion by T6SS in the progeny isolates. Such observation conveyed excessive biosynthesis of
316 alginate and suppression of T6SS in the progeny isolates during colonization. The progeny
317 isolates produce excessive alginate and exhibit more mucoid phenotype which matches with the

DEG results (Figure 5A). As alginate plays an important role in biofilm architecture and development[34], we thus quantified biofilm formation of the isolates by crystal violet staining. As seen from Figure 5B, aligned with gene expression, an increase in the biofilm formation were observed in LYSZa3 comparing to those of LYSZa2. Similarly, more biofilm formation was observed in LYSZa6 as compared to LYSZa5. RNA-seq analysis showed the adaptive changes in genes responsible for alginate biosynthesis and T6SS protein secretion in the progeny isolates.

In addition, 74 common genes in total were found to be differentially regulated in both progeny isolates, LYSZa3 and LYSZa6 (Table S8), indicating convergent gene regulation of these two isolates during colonization in different patients. Similar to the results observed from adaptive changes, most of the common genes with specific functions are involved in alginate biosynthesis and T6SS, which are the convergent changes in *P. aeruginosa* in different hosts during coinfection with SARS-CoV-2 virus. More genes were differentially regulated in LYSZa6 than LYSZa3 probably due to the longer evolving time between LYSZa5 and LYSZa6. We observed increased alginate production and elevated biofilm formation of the progeny isolates from the phenotypic assays. T6SS is used as a weapon by *P. aeruginosa* to compete with neighboring bacteria cells and to combat with the host cells in order to gain surviving advantage in the polymicrobial environment in the respiratory system. Suppression in T6SS would result in reduction in its advantage to outcompete other bacteria and its virulence to escape from host immune clearance. We thus performed bacterial competition test and cytotoxicity assay of the isolates to confirm the changes in the anti-prokaryotic and anti-eukaryotic capability between the ancestry isolates and the progeny isolates.

Decrease in bactericidal activity of *P. aeruginosa* due to suppression of T6SS

To test the reduction in the competitiveness of the progeny isolates with bacterial neighbors due

to suppression of T6SS, we examined the capability of the isolates in killing *E. coli* cells through bacterial competition assay. The isolates were mixed and cultured with *E. coli/placZ* in 1:1 ratio respectively. The mixtures were diluted to 10^{-3} while triplicate colonies of each dilution were then cultured on plate containing X-gal to test the killing efficiency (Figure 6A&B). *E. coli/pLacZ* digested X-gal and appeared as blue colonies. Survival of *E. coli* was determined both qualitatively by visualizing the intensity of blue pigment of the colonies and quantitatively by counting the blue *E. coli* CFUs left. As observed from Figure 6A&B, almost no trace of blue pigment could be observed from the mixture of the ancestry isolates, LYSZa2 and LYSZa5, with *E. coli.* More intensive blue colonies were observed from the mixed cultures of the progeny isolates, LYSZa3 and LYSZa6, with *E. coli*, indicating disadvantage of these isolates to outcompete *E. coli* comparing to their respective ancestry isolates. Same trend was also observed from quantitative tests illustrated in Figure 6C where higher numbers of *E. coli* CFU were obtained after coculturing with LYSZa3 and LYSZa6 comparing with those culturing with LYSZa2 and LYSZa5 respectively. Such results indicated a decrease in the bactericidal activity of the progeny isolates during bacterial competition consequently due to the inhibition of T6SS.

Weakened macrophage cytotoxicity of *P. aeruginosa* after T6SS suppression

We then performed macrophage killing assay to assess the decrease in cytotoxicity of the progeny isolates to eukaryotic cells upon T6SS suppression. Cultures of the isolates were added to infect macrophages individually. Relative lactate dehydrogenase (LDH) release was measured to determine the death of macrophages. More macrophages are killed, higher LDH will be released. As illustrated in Figure 7, LDH released by macrophages infected by LYSZa3 was much lower than that of LYSZa2. Similar results were observed from LYSZa5 and LYSZa6 where macrophages infected by LYSZa5 released a significant higher level of LDH comparing to

LYSZa6. LYSZa3 and LYSZa6 possess weaker cytotoxicity comparing to their ancestral isolates. Such results suggested that these *P. aeruginosa* isolates produced attenuated virulence towards their eukaryotic hosts due to the downregulation of T6SS genes after evolution.

Discussion

Upon the urgent need to prevent the spread of SARS-CoV-2 and equip people against the virus, clinical doctors and researchers put their attention on investigating the pathogenicity and epidemiology of the virus, and developing treatment measures and vaccines to combat it. However, the increased occurrence of illness and death due to bacterial coinfection and its complications indicated that there is a much underestimated and neglected influence of bacterial coinfection on the disease progression in COVID-19 patients. Here in this study, we isolated the ancestry and the progeny isolate pairs of hospital-acquired *P. aeruginosa* from two critically ill COVID-19 patients to investigate its adaptive and convergent evolution during coinfection with SARS-CoV-2 virus. We found that *P. aeruginosa* upregulates its alginate biosynthesis and downregulates its T6SS to increase its fitness in the niche and reduce its virulence to escape from host clearance for longer colonization. To the best of our knowledge, this is the first study describing the evolution of *P. aeruginosa* during coinfection with SARS-CoV-2 virus in COVID-19 patients.

The isolates collected from the two patients belongs to the same sequence type. In addition, the ancestry isolates appeared after more than 10 days of hospitalization, they are therefore hospital-acquired *P. aeruginosa* strain. Genomic sequencing analysis revealed that the genomes of the isolates carry specific GIs for DNA repair and protein secretion systems, and ARGs for multiple drug classes. Common genomic modification events identified between the progeny isolates and

386 the ancestral isolates indicated the genomic changes in genes related to T6SS, *tla3* and *tli5b3*.
387 However, no change was observed in these two genes at transcriptional level most probably due
388 to the short evolving time and the complexity of gene regulation cascades. Although the
389 expression of these two genes were not affected, we indeed observed lots of significant changes
390 at transcriptional level.

391 Through differential gene expression analysis, we found that genes involved in alginate
392 biosynthesis were upregulated greatly while genes involved in T6SS protein secretion system
393 were significantly downregulated. Alginate is an essential EPS component converting non-
394 mucoid *P. aeruginosa* to mucoid phenotype, and is important for biofilm structure and
395 antimicrobial resistance [34]. Clinical *P. aeruginosa* strains overproducing alginate isolated from
396 CF patients enhanced biofilm formation and interfered with host immune responses leading to
397 the aggravation of disease conditions and poor prognosis [35, 36]. Moreover, excessive
398 biosynthesis of alginate in *P. aeruginosa* promotes its coinfection with other pathogens such as *S.*
399 *aureus* and *B. cenocepacia* and increases their persistence in CF infections [37, 38].
400 Overproduction of alginate and increased biofilm formation were observed in the progeny strains
401 in this study, inferring the potential mechanism adopted by *P. aeruginosa* in COVID-19 patients
402 to interfere with host defense systems. Thick alginate layer is also probably a key contributing
403 factor to the increase in the antimicrobial resistance of the progeny isolate observed. Excessive
404 alginate may also facilitate coexistence of *P. aeruginosa* and other coinfecting pathogens in
405 COVID-19 for secondary bacterial infection. Further analysis is needed for deeper investigation
406 on the role of alginate in the microbial community in COVID-19 patients.

407 A more notable observation in this study is the attenuation of T6SS in the progeny isolates. The
408 expression of genes involved in T6SS protein secretion were significantly downregulated in both

409 the progeny isolates. *P. aeruginosa* T6SS functions as a phage-like toxin delivery apparatus to
410 transport toxic effectors into surrounding competing bacterial cells and also host cells to gain
411 survival advantages and invade host cells [39]. *P. aeruginosa* carries three types of T6SS, being
412 HSI-I, HSI-II, and HSI-III respectively. HSI-I is dedicated to inter-bacterial competition while
413 HSI-II and HSI-III, which are less studied, associate with both anti-prokaryotic and anti-
414 eukaryotic functions [40, 41]. Three gene clusters HSI-I, HSI-II and HSI-III contain *hcp*, *clpV*,
415 *vgrG*, *tss/his* genes and other genes including *ppkA, pppA, tag, sfa*, *fha,lip, dotU, icmF*, *stp* and
416 *stk* genes for the full function of T6SS apparatus (Figure 4)[39, 42]. In both the progeny isolates,
417 especially in LYSZa6, the expression of most of HSI-II genes and associated genes were
418 downregulated significantly (Figure 4). Such results indicated a general inhibition of HSI-II
419 T6SS in the *P. aeruginosa* isolates during convergent evolution in the patients to adapt to
420 COVID-19 environment. As HSI-II T6SS associates with anti-bacterial and anti-host functions,
421 we tested both the bacterial killing capacity and macrophage cytotoxicity of the isolates. The
422 results confirmed the decrease in the virulence to both neighbouring bacteria and host cells of the
423 progeny isolates due to reduction in T6SS expression. Previous studies had demonstrated that *P.*
424 *aeruginosa* abrogated its T6SS to adapt to the host environment by genetic modification on
425 genes such as *vgrG* and *vgrG4* during chronic infection of cystic fibrosis [16, 43]. Here we
426 showed that *P. aeruginosa* attenuated its T6SS at transcriptional level to gain fitness and survival
427 advantages during acute infection of COVID-19 pneumonia. Moreover, attenuation of T6SS in *P.*
428 *aeruginosa* may give opportunities to other bacterial pathogens to outcompete itself and making
429 host cells susceptible to subsequent infections. A recent research showed that *P. aeruginosa*
430 abrogating its T6SS could be outcompeted by coinfecting *B.cenocepaica* in CF patients in an
431 age- and T6SS-dependent manner and predisposing host to superinfection of *B.cenocepaica* [44].

P. aeruginosa attenuating its T6SS in COVID-19 patients could probably play a pivotal role in coexisting with other pathogenic strains in the polymicrobial environment and promoting subsequent infection in COVID-19 patients. Further study is indeed needed to make a deeper investigation on the role of *P. aeruginosa* played in SARS-CoV-2 infected environment. In this study, we demonstrated that *P. aeruginosa* adapted to SARS-CoV-2 infected environment by adaptive and convergent evolution in alginate biosynthesis and T6SS gene expression for enhancing biofilm formation, increasing antimicrobial resistance and gaining fitness for survival and colonization during the acute COVID-19 infection. This study will contribute to the understanding of adaptation and convergent evolution of *P. aeruginosa* which in turn helps in the precise treatment decision and novel drug target discovery to eliminate *P. aeruginosa* coinfection in COVID-19 patients.

Acknowledgements

This work was supported by Guangdong Natural Science Foundation for Distinguished Young Scholar[2020B1515020003] and Start-up Grants [Y01416106 and Y01416206] from the Southern University of Science and Technology (SUSTech) to Dr. Liang Yang, Science and Technology Program of Shenzhen [JCYJ20190809144005609] and Guangdong Basic and Applied Basic Research Foundation [2020A1515010586] to Dr. Jiuxin Qu, and Grant from Bill & Melinda Gates Foundation to Dr. Lei Liu. The authors declare that they have no competing interests.

References

1. Veras, F.P., et al., *SARS-CoV-2-triggered neutrophil extracellular traps mediate COVID-19 pathology.* J Exp Med, 2020. **217**(12).
2. Mehta, P., et al., *COVID-19: consider cytokine storm syndromes and immunosuppression.* Lancet, 2020. **395**(10229): p. 1033-1034.
3. Hanada, S., et al., *Respiratory Viral Infection-Induced Microbiome Alterations and Secondary Bacterial*

Pneumonia. Frontiers in Immunology, 2018. **9**.

4. Rawson, T.M., et al., *Bacterial and Fungal Coinfection in Individuals With Coronavirus: A Rapid Review To Support COVID-19 Antimicrobial Prescribing.* Clin Infect Dis, 2020. **71**(9): p. 2459-2468.
5. Wang, L., et al., *Coronavirus disease 2019 in elderly patients: Characteristics and prognostic factors based on 4-week follow-up.* Journal of Infection, 2020. **80**(6): p. 639-645.
6. Goyal, P., J.J. Choi, and M.M. Safford, *Clinical Characteristics of Covid-19 in New York City.* New England Journal of Medicine, 2020. **382**(24): p. 2372-2374.
7. Cox, M.J., et al., *Co-infections: potentially lethal and unexplored in COVID-19.* Lancet Microbe, 2020. **1**(1): p. e11.
8. Sharifipour, E., et al., *Evaluation of bacterial co-infections of the respiratory tract in COVID-19 patients admitted to ICU.* BMC Infect Dis, 2020. **20**(1): p. 646.
9. Zhang, G., et al., *Clinical features and short-term outcomes of 221 patients with COVID-19 in Wuhan, China.* J Clin Virol, 2020. **127**: p. 104364.
10. Shen, C., et al., *Treatment of 5 Critically Ill Patients With COVID-19 With Convalescent Plasma.* JAMA, 2020.
11. Lansbury, L., et al., *Co-infections in people with COVID-19: a systematic review and meta-analysis.* Journal of Infection, 2020. **81**(2): p. 266-275.
12. Arentz, M., et al., *Characteristics and Outcomes of 21 Critically Ill Patients With COVID-19 in Washington State.* JAMA, 2020. **323**(16): p. 1612-1614.
13. Gellatly, S.L. and R.E.W. Hancock, *Pseudomonas aeruginosa: new insights into pathogenesis and host defenses.* Pathogens and Disease, 2013. **67**(3): p. 159-173.
14. Cole, S.J., et al., *Catheter-Associated Urinary Tract Infection by Pseudomonas aeruginosa Is Mediated by Exopolysaccharide-Independent Biofilms.* Infection and Immunity, 2014. **82**(5): p. 2048-2058.
15. Wang, K., et al., *The rapid in vivo evolution of Pseudomonas aeruginosa in ventilator-associated pneumonia patients leads to attenuated virulence.* Open Biology, 2017. **7**(9).
16. Marvig, R.L., et al., *Convergent evolution and adaptation of Pseudomonas aeruginosa within patients with cystic fibrosis.* Nature Genetics, 2015. **47**(1): p. 57-+.
17. Smith, E.E., et al., *Genetic adaptation by Pseudomonas aeruginosa to the airways of cystic fibrosis patients.* Proceedings of the National Academy of Sciences of the United States of America, 2006. **103**(22): p. 8487-8492.
18. Yang, L., et al., *Evolutionary dynamics of bacteria in a human host environment.* Proceedings of the National Academy of Sciences of the United States of America, 2011. **108**(18): p. 7481-7486.
19. Wood, T.E., et al., *The Pseudomonas aeruginosa T6SS Delivers a Periplasmic Toxin that Disrupts Bacterial Cell Morphology.* Cell Reports, 2019. **29**(1): p. 187-+.
20. CLSI, *Performance Standards for Antimicrobial Susceptibility Testing. 29th ed.* CLSI supplement M100.Wayne, PA: Clinical and Laboratory Standards Institute, 2019.
21. Darling, A.E., B. Mau, and N.T. Perna, *progressiveMauve: multiple genome alignment with gene gain, loss and rearrangement.* PLoS One, 2010. **5**(6): p. e11147.
22. Larsen, M.V., et al., *Multilocus Sequence Typing of Total-Genome-Sequenced Bacteria.* Journal of Clinical Microbiology, 2012. **50**(4): p. 1355-1361.
23. Zankari, E., et al., *Identification of acquired antimicrobial resistance genes.* Journal of Antimicrobial Chemotherapy, 2012. **67**(11): p. 2640-2644.
24. Treangen, T.J., et al., *The Harvest suite for rapid core-genome alignment and visualization of thousands of intraspecific microbial genomes.* Genome Biology, 2014. **15**(11).
25. Bertelli, C., et al., *IslandViewer 4: expanded prediction of genomic islands for larger-scale datasets.* Nucleic Acids Res, 2017. **45**(W1): p. W30-W35.
26. Alikhan, N.F., et al., *BLAST Ring Image Generator (BRIG): simple prokaryote genome comparisons.* Bmc Genomics, 2011. **12**.
27. Sullivan, M.J., N.K. Petty, and S.A. Beatson, *Easyfig: a genome comparison visualizer.* Bioinformatics, 2011. **27**(7): p. 1009-10.
28. Winsor, G.L., et al., *Enhanced annotations and features for comparing thousands of Pseudomonas genomes in the Pseudomonas genome database.* Nucleic Acids Res, 2016. **44**(D1): p. D646-53.
29. Tatusova, T., et al., *NCBI prokaryotic genome annotation pipeline.* Nucleic Acids Res, 2016. **44**(14): p. 6614-24.

30. Love, M.I., W. Huber, and S. Anders, *Moderated estimation of fold change and dispersion for RNA-seq data with DESeq2.* Genome Biol, 2014. **15**(12): p. 550.
31. Huang, D.W., B.T. Sherman, and R.A. Lempicki, *Systematic and integrative analysis of large gene lists using DAVID bioinformatics resources.* Nature Protocols, 2009. **4**(1): p. 44-57.
32. Hachani, A., N.S. Lossi, and A. Filloux, *A visual assay to monitor T6SS-mediated bacterial competition.* J Vis Exp, 2013(73): p. e50103.
33. Qu, J., et al., *Persistent Bacterial Coinfection of a COVID-19 Patient Caused by a Genetically Adapted Pseudomonas aeruginosa Chronic Colonizer.* Front Cell Infect Microbiol, 2021. **11**: p. 641920.
34. Hentzer, M., et al., *Alginate overproduction affects Pseudomonas aeruginosa biofilm structure and function.* J Bacteriol, 2001. **183**(18): p. 5395-401.
35. Qiu, D., et al., *Regulated proteolysis controls mucoid conversion in Pseudomonas aeruginosa.* Proc Natl Acad Sci U S A, 2007. **104**(19): p. 8107-12.
36. Pedersen, S.S., et al., *Pseudomonas aeruginosa alginate in cystic fibrosis sputum and the inflammatory response.* Infect Immun, 1990. **58**(10): p. 3363-8.
37. Limoli, D.H., et al., *Pseudomonas aeruginosa Alginate Overproduction Promotes Coexistence with Staphylococcus aureus in a Model of Cystic Fibrosis Respiratory Infection.* mBio, 2017. **8**(2).
38. Chattoraj, S.S., et al., *Pseudomonas aeruginosa alginate promotes Burkholderia cenocepacia persistence in cystic fibrosis transmembrane conductance regulator knockout mice.* Infect Immun, 2010. **78**(3): p. 984-93.
39. Mougous, J.D., et al., *A virulence locus of Pseudomonas aeruginosa encodes a protein secretion apparatus.* Science, 2006. **312**(5779): p. 1526-30.
40. Allsopp, L.P., et al., *RsmA and AmrZ orchestrate the assembly of all three type VI secretion systems in Pseudomonas aeruginosa.* Proceedings of the National Academy of Sciences of the United States of America, 2017. **114**(29): p. 7707-7712.
41. Hachani, A., T.E. Wood, and A. Filloux, *Type VI secretion and anti-host effectors.* Curr Opin Microbiol, 2016. **29**: p. 81-93.
42. Ho, B.T., T.G. Dong, and J.J. Mekalanos, *A view to a kill: the bacterial type VI secretion system.* Cell Host Microbe, 2014. **15**(1): p. 9-21.
43. Kordes, A., et al., *Genetically diverse Pseudomonas aeruginosa populations display similar transcriptomic profiles in a cystic fibrosis explanted lung.* Nat Commun, 2019. **10**(1): p. 3397.
44. Perault, A.I., et al., *Host Adaptation Predisposes Pseudomonas aeruginosa to Type VI Secretion System-Mediated Predation by the Burkholderia cepacia Complex.* Cell Host Microbe, 2020. **28**(4): p. 534-547 e3.

Tables

		LYSZa3 vs LYSZa2				LYSZa6 vs LYSZa5			
Gene	**Product**	**Type**	**Amino acid change**	**Coding region change in longest transcript**	**Non-synonymous**	**Type**	**Amino acid change**	**Coding region change in longest transcript**	**Non-synonymous**
PA0041	hemagglutinin	SNV		5803C>T	No	SNV		5803C>T	No
PA0259	Type 6 lipase adaptor, Tla3	SNV		333A>G	No	SNV		333A>G	No
		MNV		330_331delinsTT	No	MNV		330_331delinsTT	No
		SNV		327T>G	No	SNV		327T>G	No
		SNV		324T>A	No	SNV		324T>A	No

		MNV	Ser107Asn	320_321delinsAT	Yes	MNV	Ser107Asn	320_321delinsAT	Yes
		SNV		315T>C	No	SNV		315T>C	No
		SNV	Asp105Asn	313G>A	Yes	SNV	Asp105Asn	313G>A	Yes
		SNV		303G>A	No	SNV		303G>A	No
fiuA	ferrichrome receptor FiuA	SNV		1854C>T	No	SNV		1854C>T	No
		SNV		1842G>C	No	SNV		1842G>C	No
		SNV		1830G>C	No	SNV		1830G>C	No
		SNV	Ile608Met	1824C>G	Yes	SNV	Ile608Met	1824C>G	Yes
		SNV	Ile608Leu	1822A>C	Yes	SNV	Ile608Leu	1822A>C	Yes
		SNV		1812G>A	No	SNV		1812G>A	No
		SNV		1800G>C	No	SNV		1800G>C	No
		SNV		1797G>A	No	SNV		1797G>A	No
		SNV		1794G>C	No	SNV		1794G>C	No
		SNV		1792C>T	No	SNV		1792C>T	No
		Deletion	Ser597fs	1790delC	Yes	Deletion	Ser597fs	1790delC	Yes
		SNV	Ser596Arg	1788T>A	Yes	SNV	Ser596Arg	1788T>A	Yes
		Insertion	Ser596fs	1786dupA	Yes	Insertion	Ser596fs	1786dupA	Yes
		SNV	Thr595Asn	1784C>A	Yes	SNV	Thr595Asn	1784C>A	Yes
		MNV		1780_1781delinsTC	No	MNV		1780_1781delinsTC	No
		Insertion	Asn593fs	1778_1779insGG	Yes	Insertion	Asn593fs	1778_1779insGG	Yes
		MNV	Met592_Asn593delinsIleTyr	1776_1777delinsAT	Yes	MNV	Met592_Asn593delinsIleTyr	1776_1777delinsAT	Yes
		Replacement	Met592fs	1773delinsCG	Yes	Replacement	Met592fs	1773delinsCG	Yes
PA4514	iron transport outer membrane	SNV	Thr193Ile	578C>T	Yes	SNV	Thr193Ile	578C>T	Yes
		Replacement	Asp190fs	569_570delinsG	Yes	Replacement	Asp190fs	569_570delinsG	Yes

	receptor	SNV	Gln189Leu	566A>T	Yes	SNV	Gln189Leu	566A>T	Yes
		Insertion	Gln189fs	564dupG	Yes	Insertion	Gln189fs	564dupG	Yes
PA5088	type VI secretion lipase immunity protein, Tli5b3	SNV	Gly181Ser	541G>A	Yes	SNV	Gly181Ser	541G>A	Yes
		SNV		528G>C	No	SNV		528G>C	No

542 **Table 1.** Common genetic mutations identified between LYSZa3 and LYSZa6. Full list of
543 genetic mutations is included in Table S5.

Gene	Product Name	Base Mean	Fold Change	Adj.p-value	LYSZa2 Mean	LYSZa3 Mean
algD	GDP-mannose 6-dehydrogenase AlgD	27877.94	1091.52	0.00E+00	61.33	50065.00
algX	alginate biosynthesis protein AlgX	1967.25	256.42	2.31E-236	18.33	3478.67
algA	phosphomannose isomerase / guanosine 5'-diphospho-D-mannose pyrophosphorylase	5853.40	238.02	0.00E+00	59.00	10382.00
algE	Alginate production outer membrane protein AlgE precursor	2204.36	221.80	3.29E-252	24.00	3889.33
algF	alginate o-acetyltransferase AlgF	1648.75	211.59	3.00E-242	18.67	2924.00
algL	poly(beta-d-mannuronate) lyase precursor AlgL	2134.58	182.28	4.64E-245	28.00	3766.33
alg44	alginate biosynthesis protein Alg44	1855.41	162.63	1.64E-285	27.33	3260.33
algJ	alginate o-acetyltransferase AlgJ	1033.36	154.76	2.12E-191	16.00	1783.33
algK	alginate biosynthetic protein AlgK precursor	1171.78	145.20	2.18E-233	19.33	2043.00
alg8	alginate biosynthesis protein Alg8	2758.04	133.33	0.00E+00	49.67	4939.33
algI	alginate o-acetyltransferase AlgI	1457.21	59.29	1.83E-259	58.33	2501.67
algG	alginate-c5-mannuronan-epimerase AlgG	1682.20	16.89	1.73E-125	226.00	2793.33
hcpB	secreted protein Hcp	107.95	-4.46	1.17E-20	215.67	36.00
PA1663	Sfa2	305.43	-4.46	2.74E-47	603.33	100.00

PA1666	Lip2	159.33	-4.50	2.97E-24	319.00	52.67
PA2362	DotU3	22.49	-4.54	4.95E-06	44.00	7.00
PA1660	HsiG2	346.81	-4.63	1.56E-59	686.67	110.33
PA1662	clpV2	1014.01	-4.63	3.41E-44	2020.67	318.00
PA1661	HsiH2	246.25	-4.65	1.19E-39	488.33	77.67
PA1659	HsiF2	163.52	-5.59	1.38E-34	334.00	43.00
PA1657	HsiB2	842.21	-6.21	6.69E-109	1743.67	204.33
PA1658	HsiC2	1839.66	-6.47	4.92E-141	3824.67	437.00
PA2364	Lip3	32.22	-9.20	6.01E-13	70.33	5.67

Table 2. Selected DEGs in LYSZa3 comparing to LYSZa2 related to alginate biosynthesis and Type VI secretion system. Filtering criteria are fold change ≧4, adjusted p-value<0.05 and base mean ≧ 20. Full list of DEGs is included in Table S6.

Gene	Product Name	Base Mean	Fold Change	Adj. p-value	LYSZa2 Mean	LYSZa3 Mean
algD	GDP-mannose 6-dehydrogenase AlgD	2956.90	138.79	2.47E-170	39.33	6375.00
algX	alginate biosynthesis protein AlgX	271.80	45.97	1.05E-75	10.67	585.67
algL	poly(beta-d-mannuronate) lyase precursor AlgL	283.61	44.85	1.98E-74	11.33	609.00
algJ	alginate o-acetyltransferase AlgJ	118.03	32.97	3.93E-33	6.33	248.67
algE	Alginate production outer membrane protein AlgE precursor	254.48	25.19	1.11E-61	18.33	535.33
algA	phosphomannose isomerase / guanosine 5'-diphospho-D-mannose pyrophosphorylase	481.88	21.52	9.22E-64	39.00	1000.67
algF	alginate o-acetyltransferase AlgF	152.00	18.68	7.50E-42	14.33	314.67
alg8	alginate biosynthesis protein Alg8	292.51	14.91	1.09E-59	34.67	599.33
alg44	alginate biosynthesis protein Alg44	195.56	14.43	3.38E-61	23.67	403.00
algK	alginate biosynthetic protein AlgK precursor	135.65	10.35	6.37E-39	21.67	272.67
algI	alginate o-acetyltransferase AlgI	218.14	8.40	7.47E-47	43.00	427.33

algG	alginate-c5-mannuronan-epimerase AlgG	356.62	4.45	4.15E-53	121.33	644.33
clpV1	ClpV1	5315.67	-4.08	7.48E-33	7854.33	2309.33
PA3904	PAAR4	1457.06	-4.17	3.79E-33	2178.00	631.67
PA2702	Tse2	280.90	-4.35	2.50E-29	419.33	117.33
PA2774	Tse4	296.61	-4.37	4.85E-26	461.67	122.33
PA2775	Tsi4	133.81	-4.71	7.24E-19	212.67	52.33
vgrG1	VgrG1	2637.35	-4.74	1.56E-50	3969.33	1016.67
PA0093	Tse6	947.79	-4.91	3.88E-46	1469.00	360.00
PA3905	type VI effector chaperone for Tox-Rease, TecT	1073.56	-4.95	1.10E-53	1671.00	403.00
PA0082	TssA1	1449.46	-5.32	1.76E-55	2265.00	515.00
PA2703	Tsi2	98.26	-5.56	5.99E-24	156.67	33.00
PA0094	EagT6	251.06	-5.79	1.43E-38	401.67	82.00
PA3484	Tse3	544.56	-5.86	1.50E-54	869.33	174.33
stk1	Stk1	263.85	-5.90	1.38E-56	423.00	84.67
PA5266	VgrG6	396.48	-6.81	6.50E-47	654.33	113.33
PA1667	HsiJ2	678.54	-6.99	2.41E-100	1119.67	188.67
PA1656	HsiA2	3257.03	-7.01	4.84E-80	5349.67	911.33
PA1662	clpV2	2538.08	-8.98	3.88E-108	4332.33	564.33
PA1661	HsiH2	693.51	-9.91	1.55E-110	1186.67	142.00
PA1666	Lip2	340.97	-10.48	2.48E-72	589.00	65.67
stp1	Stp1	327.95	-10.61	1.67E-70	562.67	62.67
hcpA	secreted protein Hcp	72.34	-10.75	7.25E-26	125.33	13.67
PA1665	Fha2	840.73	-10.96	1.12E-108	1456.67	155.33
PA1660	HsiG2	907.03	-11.05	1.78E-125	1551.67	167.33
PA1669	IcmF2	2052.74	-11.08	6.20E-107	3547.33	375.67
hcpB	secreted protein Hcp	204.27	-11.30	8.81E-47	358.00	36.67
PA1668	DotU2	487.58	-11.30	1.39E-105	836.33	88.00
PA1663	Sfa2	883.17	-12.92	4.47E-74	1556.67	139.33
PA3334	Acp3	236.04	-13.79	1.82E-73	415.67	35.33
PA1657	HsiB2	2539.11	-14.39	1.32E-112	4445.00	366.00

PA1659	HsiF2	480.65	-17.06	4.25E-89	843.33	59.00
PA1658	HsiC2	5746.91	-17.11	4.82E-66	10179.00	695.67

Table 3. Selected DEGs in LYSZa6 comparing to LYSZa5 related to alginate biosynthesis and Type VI secretion system. Filtering criteria are fold change ≧4, adjusted p-value<0.05 and base mean ≧ 20. Full list of DEGs is included in Table S7.

Figure legends

Figure 1. Ring Plot and Phylogenetic tree of LYSZa2 and LYSZa5. **(A)**Ring plot of LYSZa2 and LYSZa5 comparing with other *P. aeruginosa* genomes. From the innermost, ring 1: GC content (black); ring 2: GC skew (purple/green); ring 3: LYSZa2(dark red); ring 4: LYSZa5(navy); ring 5: PAO1 lab reference strain (violet); ring 6: PA14 clinical virulent strain (orange); ring 7: LESB58 hypervirulent clinical strain from CT patient (olive); ring 8: SCV20265 small colony variant strain (light green); ring 9: VRFPA04 multidrug resistant strain from keratitis patient(cyan); ring 10&11: GIs on LYSZa2 and LYSZa5 (black); ring 12&13: ARGs on LYSZa2 and LYSZa5 (red); **(B)** phylogenetic tree constructed using LYSZa2 and LYSZa5 genomes and 23 other *P. aeruginosa* genomes based on core genome alignment, LYSZa2 and LYSZa5 are highlighted in red.

Figure 2. Heatmaps and PCoA plots of DEGs between the ancestry isolates and the progeny isolates. **(A)** heatmap of significant DEGs in LYSZa3 comparing to LYSZa2; **(B)** heatmap of significant DEGs in LYSZa6 comparing to LYSZa5; **(C)** PCoA plots of LYSZa3 group and LYSZa2 group based on DEGs using Bray Curtis dissimilarity; **(D)** PCoA plots of LYSZa6 group and LYSZa5 group based on DEGs using Bray Curtis dissimilarity.

Figure 3. GO enrichment analysis and variation in gene abundance in each GO. **(A)** GO enriched

569 in LYSZa3 comparing to LYSZa2, bars towards right-hand side showing genes assigned to the
570 functions were upregulated, bars towards left-hand side showing genes assigned to the functions
571 were downregulated, up- and down-regulation are indicated in the legend as well, p-value < 0.05;
572 **(B)** Variation in gene abundance involved in the enriched GO functions listed in A in LYSZa2
573 and LYSZa3; **(C)** GO enriched in LYSZa6 comparing to LYSZa5, bars towards right-hand side
574 showing genes assigned to the functions were upregulated, bars towards left-hand side showing
575 genes assigned to the functions were downregulated, up- and down-regulation are indicated in
576 the legend as well, p-value < 0.05; **(D)** Variation in gene abundance involved in the enriched GO
577 functions listed in C in LYSZa5 and LYSZa6.
578
579 **Figure 4.** Schematic figure of HSI-I, HSI-II and HSI-III gene clusters. Genes downregulated in
580 LYSZa3 are denoted by purple crosses; genes downregulated in LYSZa6 are denoted by red
581 triangles. Gene name was obtained from Pseudomonas Genome Database [49].
582
583 **Figure 5**. Phenotypic analysis. **(A)** Colony morphologies of the isolates; **(B)** Biofilm
584 quantification tests by crystal violet staining, **: p-value < 0.05; Upper panel: biofilm
585 quantification test of LYSZa2 and LYSZa3, lower panel: biofilm quantification test of LYSZa5
586 and LYSZa6.
587
588 **Figure 6.** Bacterial competition assay between the isolates and *E. coli.* Blue pigment intensity
589 indicates the survival of *E. coli.***(A)** Upper panel: competition between LYSZa2 and *E. coli*;
590 lower panel: competition between LYSZa3 and *E. coli*, number in each section denotes the
591 dilution factor, ranged from 10^0 to 10^{-3}; **(B)** Upper panel: competition between LYSZa5 and *E.*
592 *coli*; lower panel: competition between LYSZa6 and *E. coli*, number in each section denotes the

593 dilution factor, ranged from 10^0 to 10^{-3}; **(C)** Counts of *E. coli* CFU left in each competition, **:

594 p-value<0.05.

595

596

597 **Figure 7.** Macrophage cytotoxicity assay of the ancestry isolates and the progeny isolates.

598 Killing of macrophage is illustrated by the percent of LDH released, **: p-value<0.05.

599

600

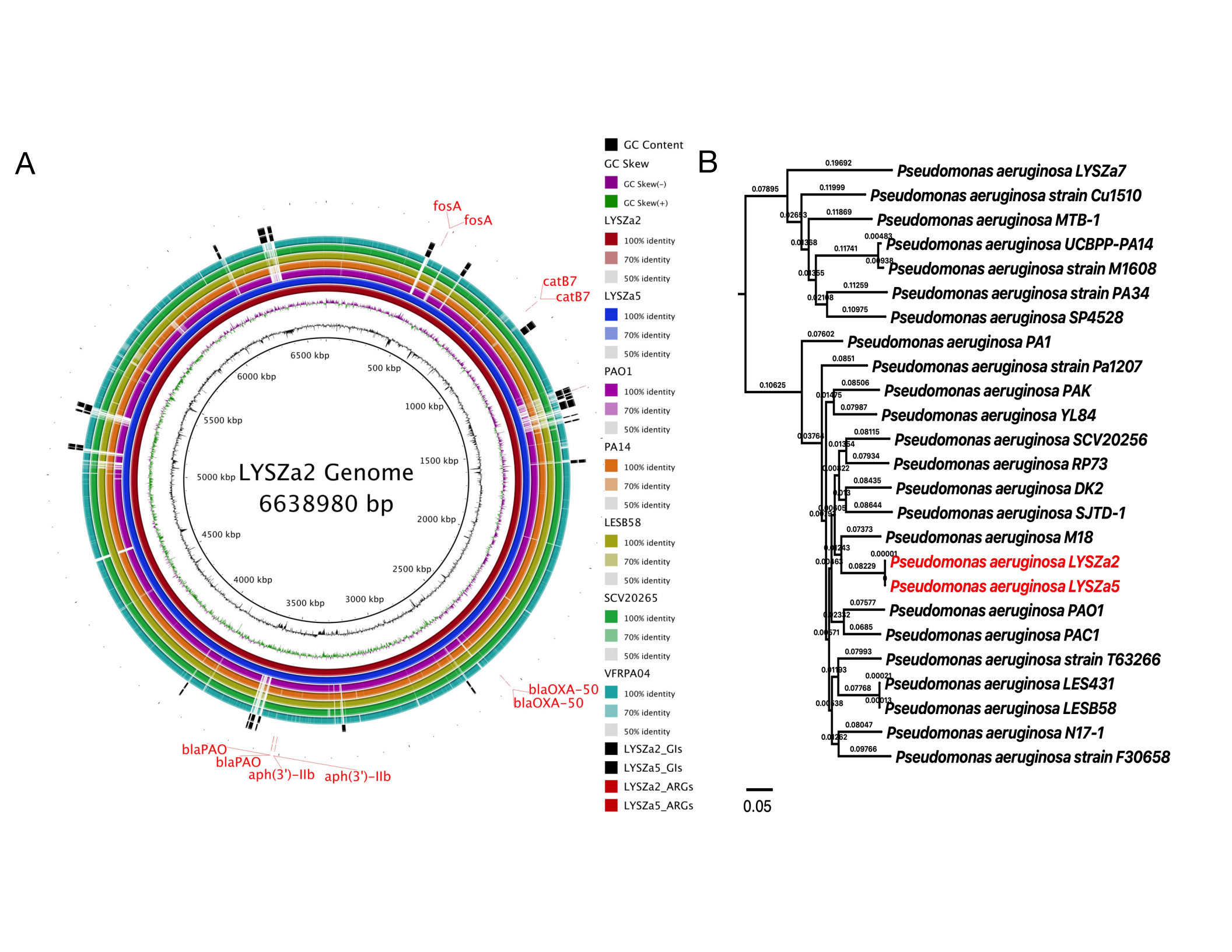
A
fosA
fosA
catB7
catB7
6500 kbp
500 kbp
6000 kbp
1000 kbp
5500 kbp
1500 kbp
5000 kbp
LYSZa2 Genome
6638980 bp
2000 kbp
4500 kbp
2500 kbp
4000 kbp
3500 kbp
3000 kbp
blaOXA-50
blaOXA-50
blaPAO
blaPAO
aph(3')-IIb
aph(3')-IIb
GC Content
GC Skew
GC Skew(-)
GC Skew(+)
LYSZa2
100% identity
70% identity
50% identity
LYSZa5
100% identity
70% identity
50% identity
PAO1
100% identity
70% identity
50% identity
PA14
100% identity
70% identity
50% identity
LESB58
100% identity
70% identity
50% identity
SCV20265
100% identity
70% identity
50% identity
VFRPA04
100% identity
70% identity
50% identity
LYSZa2_GIs
LYSZa5_GIs
LYSZa2_ARGs
LYSZa5_ARGs
B
0.19692
Pseudomonas aeruginosa LYSZa7
0.07895
0.11999
Pseudomonas aeruginosa strain Cu1510
0.11869
Pseudomonas aeruginosa MTB-1
0.00483
Pseudomonas aeruginosa UCBPP-PA14
0.11741
Pseudomonas aeruginosa strain M1608
0.11259
Pseudomonas aeruginosa strain PA34
0.10975
Pseudomonas aeruginosa SP4528
0.07602
Pseudomonas aeruginosa PA1
0.0851
Pseudomonas aeruginosa strain Pa1207
0.10625
0.08506
Pseudomonas aeruginosa PAK
0.07987
Pseudomonas aeruginosa YL84
0.08115
Pseudomonas aeruginosa SCV20256
0.07934
Pseudomonas aeruginosa RP73
0.08435
Pseudomonas aeruginosa DK2
0.08644
Pseudomonas aeruginosa SJTD-1
0.07373
Pseudomonas aeruginosa M18
0.00001
Pseudomonas aeruginosa LYSZa2
0.08229
Pseudomonas aeruginosa LYSZa5
0.07577
Pseudomonas aeruginosa PAO1
0.0685
Pseudomonas aeruginosa PAC1
0.07993
Pseudomonas aeruginosa strain T63266
0.00021
Pseudomonas aeruginosa LES431
0.07768
0.00013
Pseudomonas aeruginosa LESB58
0.08047
Pseudomonas aeruginosa N17-1
0.09766
Pseudomonas aeruginosa strain F30658
0.05

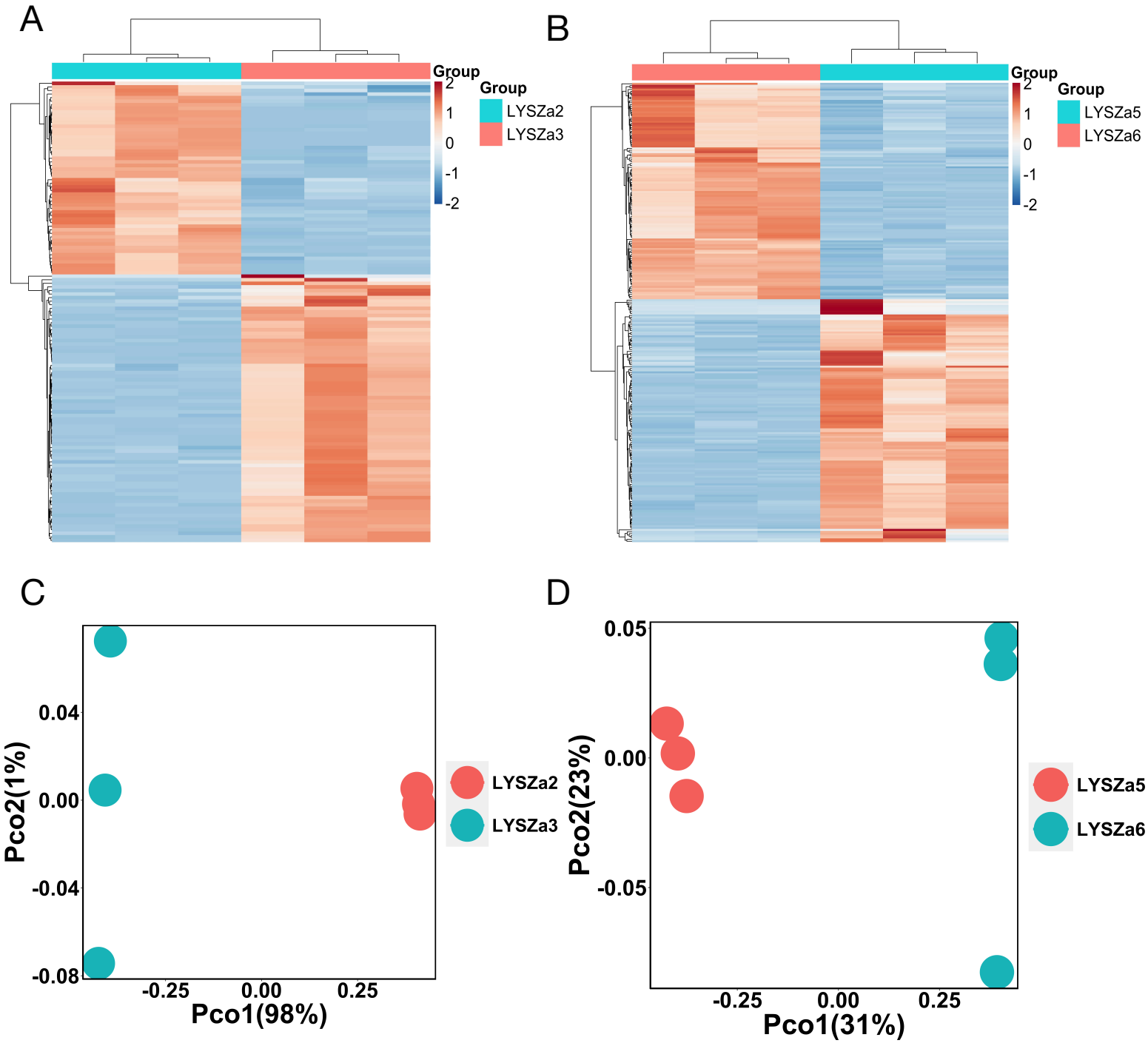
A
Group
2
1
0
-1
-2
Group
LYSZa2
LYSZa3
B
Group
2
1
0
-1
-2
Group
LYSZa5
LYSZa6
C
0.04
0.00
-0.04
-0.08
Pco2(1%)
-0.25
0.00
0.25
Pco1(98%)
LYSZa2
LYSZa3
D
0.05
0.00
-0.05
Pco2(23%)
-0.25
0.00
0.25
Pco1(31%)
LYSZa5
LYSZa6

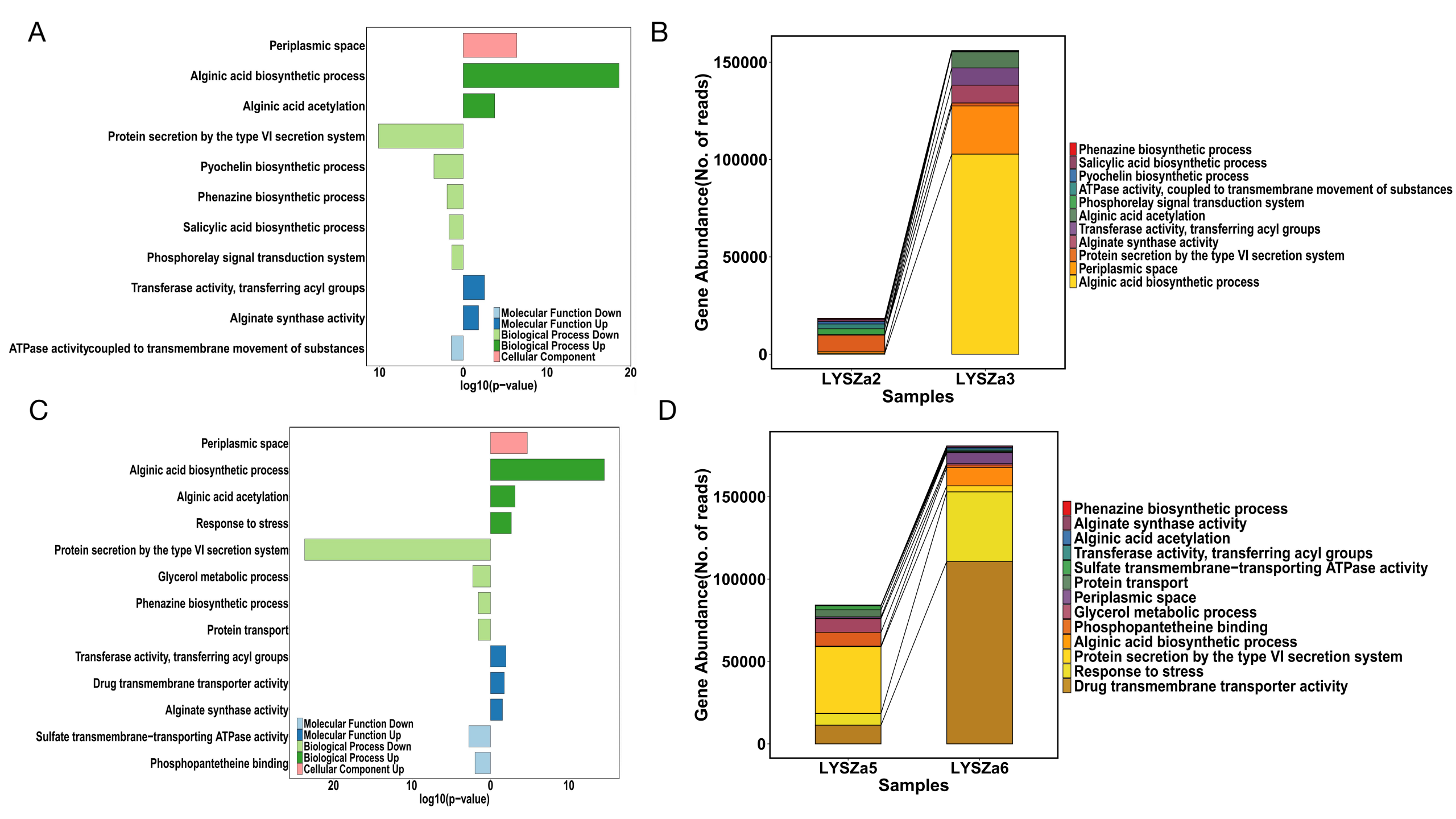
A
Periplasmic space
Alginic acid biosynthetic process
Alginic acid acetylation
Protein secretion by the type VI secretion system
Pyochelin biosynthetic process
Phenazine biosynthetic process
Salicylic acid biosynthetic process
Phosphorelay signal transduction system
Transferase activity, transferring acyl groups
Alginate synthase activity
ATPase activitycoupled to transmembrane movement of substances
Molecular Function Down
Molecular Function Up
Biological Process Down
Biological Process Up
Cellular Component
10
0
10
20
log10(p-value)
B
Gene Abundance(No. of reads)
150000
100000
50000
0
LYSZa2
LYSZa3
Samples
Phenazine biosynthetic process
Salicylic acid biosynthetic process
Pyochelin biosynthetic process
ATPase activity, coupled to transmembrane movement of substances
Phosphorelay signal transduction system
Alginic acid acetylation
Transferase activity, transferring acyl groups
Alginate synthase activity
Protein secretion by the type VI secretion system
Periplasmic space
Alginic acid biosynthetic process
C
Periplasmic space
Alginic acid biosynthetic process
Alginic acid acetylation
Response to stress
Protein secretion by the type VI secretion system
Glycerol metabolic process
Phenazine biosynthetic process
Protein transport
Transferase activity, transferring acyl groups
Drug transmembrane transporter activity
Alginate synthase activity
Sulfate transmembrane-transporting ATPase activity
Phosphopantetheine binding
Molecular Function Down
Molecular Function Up
Biological Process Down
Biological Process Up
Cellular Component Up
20
10
0
10
log10(p-value)
D
Gene Abundance(No. of reads)
150000
100000
50000
0
LYSZa5
LYSZa6
Samples
Phenazine biosynthetic process
Alginate synthase activity
Alginic acid acetylation
Transferase activity, transferring acyl groups
Sulfate transmembrane-transporting ATPase activity
Protein transport
Periplasmic space
Glycerol metabolic process
Phosphopantetheine binding
Alginic acid biosynthetic process
Protein secretion by the type VI secretion system
Response to stress
Drug transmembrane transporter activity

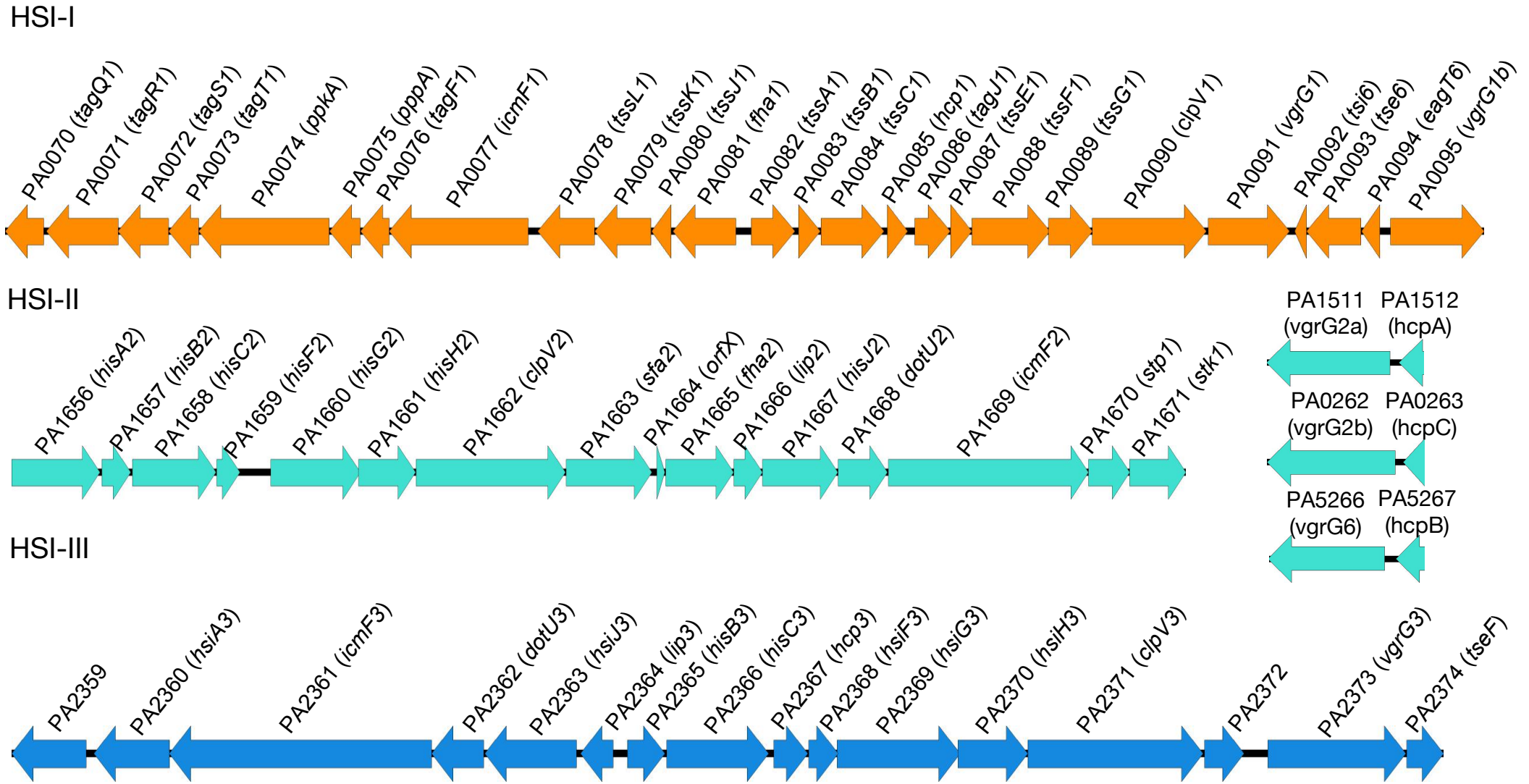
HSI-I
PA0070 (tagQ1)
PA0071 (tagR1)
PA0072 (tagS1)
PA0073 (tagT1)
PA0074 (ppkA)
PA0075 (pppA)
PA0076 (tagF1)
PA0077 (icmF1)
PA0078 (tssL1)
PA0079 (tssK1)
PA0080 (tssJ1)
PA0081 (fha1)
PA0082 (tssA1)
PA0083 (tssB1)
PA0084 (tssC1)
PA0085 (hcp1)
PA0086 (tagJ1)
PA0087 (tssE1)
PA0088 (tssF1)
PA0089 (tssG1)
PA0090 (clpV1)
PA0091 (vgrG1)
PA0092 (tsi6)
PA0093 (tse6)
PA0094 (eagT6)
PA0095 (vgrG1b)
HSI-II
PA1656 (hisA2)
PA1657 (hisB2)
PA1658 (hisC2)
PA1659 (hisF2)
PA1660 (hisG2)
PA1661 (hisH2)
PA1662 (clpV2)
PA1663 (sfa2)
PA1664 (orfX)
PA1665 (fha2)
PA1666 (lip2)
PA1667 (hisJ2)
PA1668 (dotU2)
PA1669 (icmF2)
PA1670 (stp1)
PA1671 (stk1)
PA1511 (vgrG2a)
PA1512 (hcpA)
PA0262 (vgrG2b)
PA0263 (hcpC)
PA5266 (vgrG6)
PA5267 (hcpB)
HSI-III
PA2359
PA2360 (hsiA3)
PA2361 (icmF3)
PA2362 (dotU3)
PA2363 (hsiJ3)
PA2364 (lip3)
PA2365 (hisB3)
PA2366 (hisC3)
PA2367 (hcp3)
PA2368 (hsiF3)
PA2369 (hsiG3)
PA2370 (hsiH3)
PA2371 (clpV3)
PA2372
PA2373 (vgrG3)
PA2374 (tseF)

A

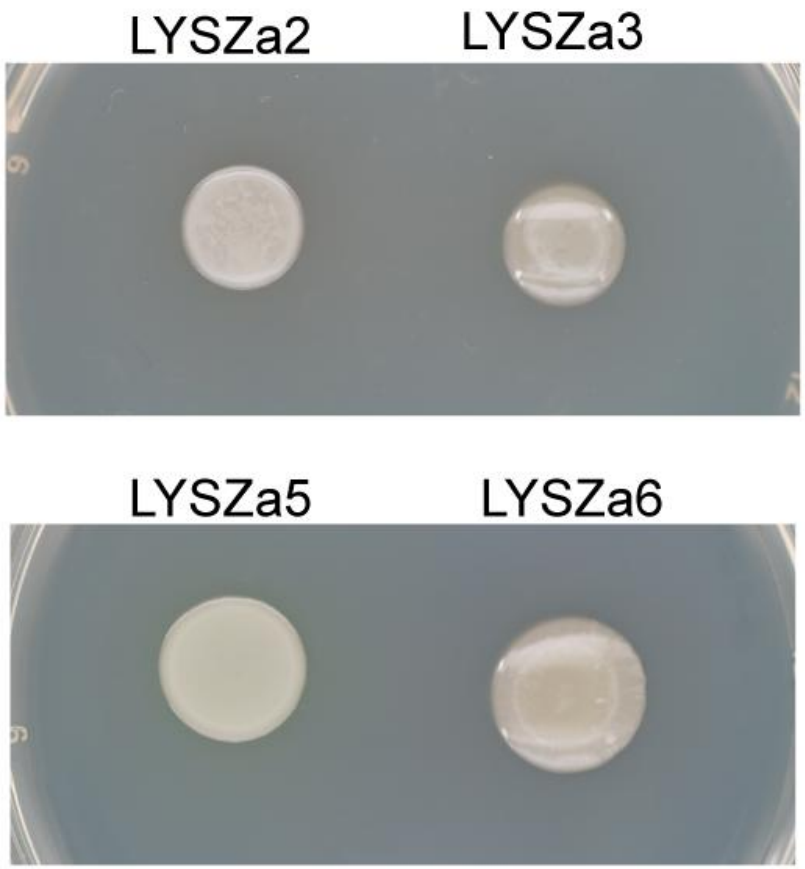
LYSZa2
LYSZa3
LYSZa5
LYSZa6

B

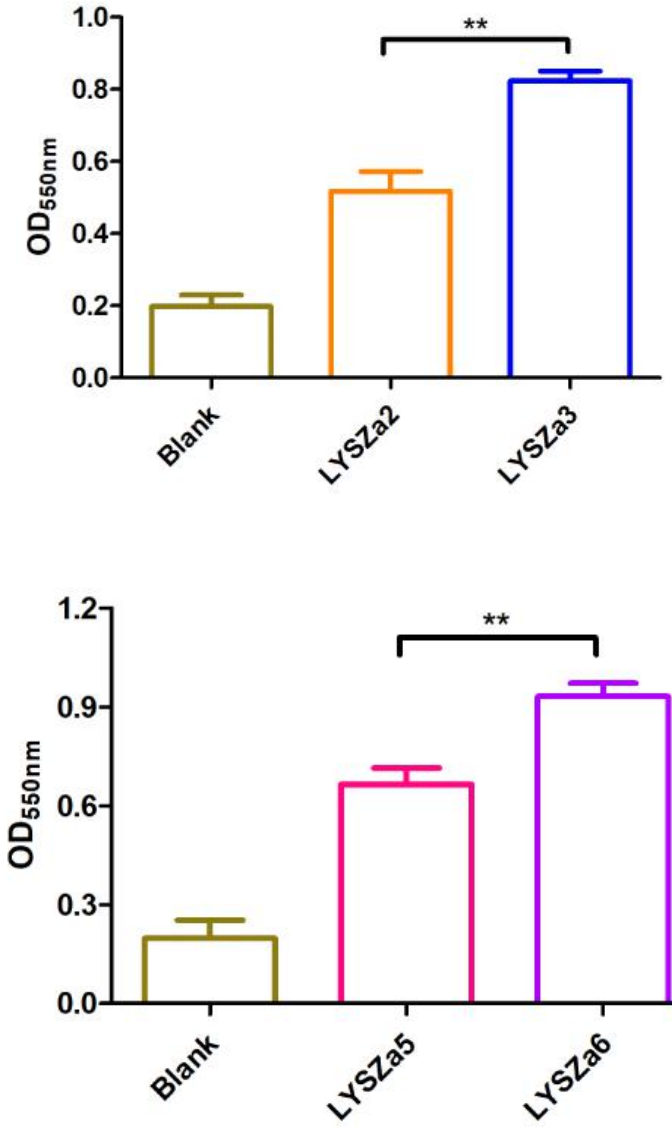
1.0
0.8
0.6
0.4
0.2
0.0
OD550nm
**
Blank
LYSZa2
LYSZa3
1.2
0.9
0.6
0.3
0.0
OD550nm
**
Blank
LYSZa5
LYSZa6

A

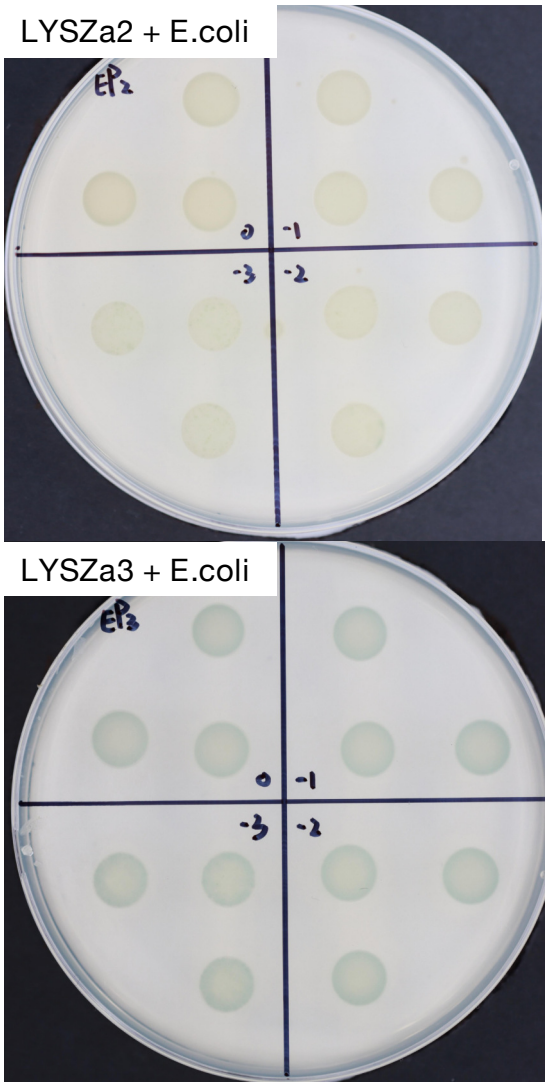
LYSZa2 + E.coli
LYSZa3 + E.coli

B

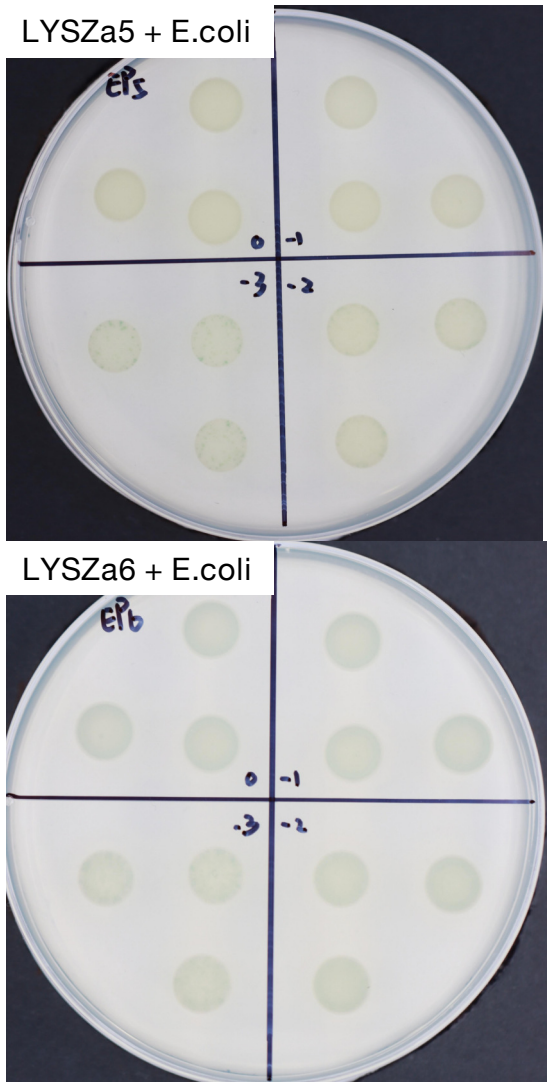
LYSZa5 + E.coli
LYSZa6 + E.coli

C

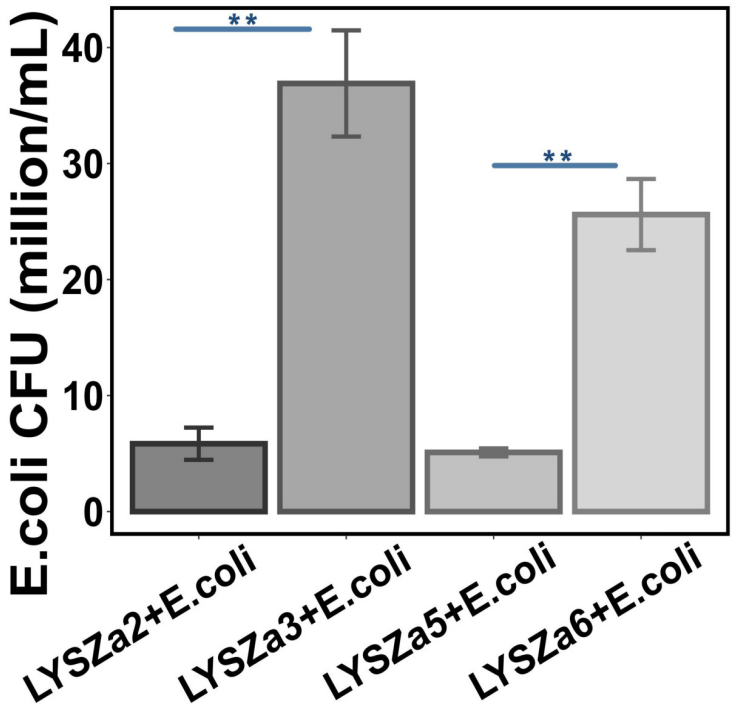
E.coli CFU (million/mL)
0
10
20
30
40
**
**
LYSZa2+E.coli
LYSZa3+E.coli
LYSZa5+E.coli
LYSZa6+E.coli